Behavior of the 9-Anthryl-*tert*-butylcarbinol as a Chiral Solvating Agent. Study of Diastereochemical Association by Intermolecular NOE and Molecular Dynamics Calculations

M. de Moragas,[†] E. Cervelló,[†] A. Port,[†] C. Jaime,[†] A. Virgili,*[,†] and B. Ancian[‡]

Unitat de Química Orgànica, Departament de Química, Universitat Autònoma de Barcelona, 08193 Bellaterra, Barcelona, Spain, and Department of Chemistry, Université Paris 7, Place Jussieu, 75251 Paris Cedex 05, France

Received February 12, 1998

The 9-anthryl-*tert*-butylcarbinol was tested as a chiral solvating agent (CSA) in the presence of racemic forms of mentil-*p*-toluenesulfinate, 9-(1-amino-2,2-dimethylpropyl)-9,19-dihydroanthracene, α-methoxyphenylacetic acid and 1-phenyl-1,2-ethanediol. Diastereomeric complexes were found to form between each enantiomer of these last two compounds. One of the enantiomers of 9-anthryl-*tert*-butylcarbinol was studied by means of intermolecular NOE and molecular dynamics calculations. Major thermodynamic and structural differences were found.

Introduction

The homochiral preparation of 9-anthryl-*tert*-butylcarbinol (**1**) from its ketone derivative, 9-pivaloylanthracene, has recently been reported.[1] Compound **1** might be useful for inducing chirality in cycloaddition reactions (such as Diels−Alder[2]) or in dipolar condensations.[3] The preparation of 9-(1-amino-2,2-dimethylpropyl)-9,10-dihydroanthracene (**2**) from its imino derivative has also been described.[4] Compound **2**, in its homochiral form, behaved like a chiral solvating agent (CSA).

The conformational study of **1** showed a very high rotational barrier (22 kcal/mol)[5] around the sp^3-sp^3 C_9-C_{11} bond. This rotation and the acidity of the benzylic proton are essential factors[6] for chiral discriminatory ability by complex formation.

The nuclear Overhauser effect[7] (NOE) is one of the main techniques used in studying the configuration and conformation of molecules in solution. The intermolecular[8] version of NOE enables several interatomic distances to be correlated in various molecules. However, this is only possible in the condition in which the formation of a solvating complex is favorable (thermodynamic factor) and/or when the molecules are near for enough time (kinetic factor) to carry out the mechanisms of intermolecular transversal relaxation. In the host−guest complexes,[9] the intermolecular NOE can confirm definitively inclusion complex formation as well as its 3-D geometry.

Scheme 1

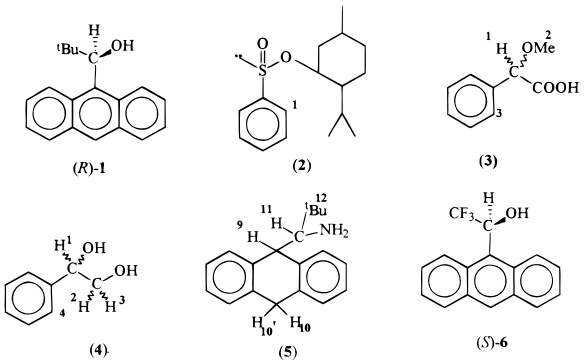

The use of hydrogen bonds and π,π-stacking interactions as complexation forces in molecular recognition is of particular interest in the separation and analysis of enantiomers in partially enriched or racemic mixtures. The chiral recognition of the *N*-(2-naphthyl)alanine methyl ester and the *N*-(3,5-dinitrobenzoyl)leucine propylamide was studied by Pirkle and co-workers[10] using NMR, chromatographic, and X-ray methods, producing similar results. 4-(3,5-Dinitrobenzamido)tetrahydrophenanthrene, the compound responsible for the chiral separation activity of the commercially available Welch-O1[11] HPLC column, was also studied via intermolecular NOE.[12]

In this paper, the capacity of compound **1** to act as a CSA is studied, and also, we try to define the nature of the intermolecular interactions that produce the enantiodifferentiation by NOE methods and theoretical calculations. We compare the results obtained for the cited compound with those obtained for the Pirkle alcohol.

[†] Universitat Autònoma de Barcelona.

[‡] Department of Chemistry, Universitè Paris 7.

(1) Moragas, M.; Port, A.; Sanchez-Ruiz, X.; Jaime, C.; Roussel, C.; Virgili, A. *Tetrahedron*: *Asymmetry* **1995**, *6*, 1307.

(2) Carrière, A.; Virgili, A. *Tetrahedron: Asymmetry* **1996**, *7*, 227.

(3) Carrière, A.; Virgili, A.; Figueredo, M. *Tetrahedron Asymmetry* **1996**, *7*, 2793.

(4) Port, A.; Jaime, C.; Virgili, A. *Tetrahedron Asymmetry* **1996**, *7*, 1295.

(5) Riggi, I.; Virgili, A.; de Moragas, M.; Jaime, C. *J. Org. Chem.* **1995**, *60*, 27.

(6) Pirkle, W. H.; Finn, J. M. *J. Org. Chem.* **1981**, *46*, 2935. (b) Rzepa, S.; Webb, M. L.; Slawin, M. Z.; Williams, D. J. *J. Chem. Soc., Chem. Commun.* **1991**, 765.

(7) Neuhaus, D.; Williamson, M. P. *The Nuclear Overhauser Effect in Estructural and Conformational Analisys*; VCH Pubblishers, Inc.: New York, 1989.

(8) Mo, H.; Pochapsky, T. C. *Nucl. Magn. Reson. Spectrosc.* 1997, *30*, 1.

(9) Jaime, C.; Redondo, J.; Sánchez-Ferrando, F.; Virgili, A. *J. Org. Chem.* **1990**, *55*, 5227.

(10) Pirkle, W. H.; Pochapsky, T. C. *J. Am. Chem. Soc.* **1986**, *108*, 5627.

(11) Regis Technologies, Inc., 8210 N., Austin Ave., Morton Grove, IL 60053-0519.

(12) Pirkle, W. H. Selness, S. R. *J. Org. Chem.* **1995**, *60*, 3252.

(13) Pirkle, W. H.; Pochapsky, T. C. *J. Am. Chem. Soc.* **1987**, *109*, 5975.

(14) Johnson, C. E.; Bovey, F. A. *J. Chem. Phys.* **1958**, *41*, 3277. (b) Waugh, J. S. Fessenden, R. W. *J. Am. Chem. Soc.* **1957**, *79*, 846.

10.1021/jo980261f CCC: $15.00
Published on Web 11/10/1998

Table 1. Measurement of the Maximum Induced Chemical Shift on Racemic Compounds 2−5 Using (*R*)-1 and Pirkle's Alcohol as CSA

			addition of (*R*)-**1**		addition of (*S*)-**6**	
entry	compound	observed resonance	maximum Δδ/ppm	r^a	maximum Δδ/ppm	r^a
7	**2**	H-9	0.020	1.2	0.028	1.2
8		H-10	0.010	1.2	0	1.2
9		H-11	0.020	1.2	0.075	1.2
10		^{t}Bu-12	0.030	1.2	0.066	1.2
2	**2**	H-1	0.010	2.0	0.010	0.9
3		(CH_3)-2	0.009	2.0	0.007	0.9
4	**4**	H-1	0.010	1.5	0.035	1.2
5		H-2	0.003	1.5	0.020	1.2
6		H-3	0.012	1.5	0.020	1.2
1	**5**	H-1	0.003	1.2	0.023	1.2

[a] Relationship between CSA and compound.

Results

Chiral Induction Activity. Compound **1** was prepared as described,[5] and its enantiomers were separated in a medium pressure HPLC system using a triacetyl cellulose column.[1]

Substrate **1** was tested as a CSA in the presence of several racemic and nonracemic chiral compounds. Its association with four species was studied: 9-(1-amino-2,2-dimethylpropyl)-9,10-dihydroanthracene (**2**), (α)-methylphenylacetic acid (**3**), 1-phenyl-1,2-ethanediol (**4**), and methyl *p*-toluenesulfinate (**5**) (Scheme 1).

The formation of the complexes was confirmed by the observation of the duplicity of most of the NMR signals. The addition of the increasing amounts of (*R*)-**1** to each compound allowed us to calibrate the maximum difference in the chemical shift thus induced. Enantiomeric purity was measured by integrating several absorptions. The measurement was repeated using Pirkle's alcohol (**6**). Results are shown in Table 1.

In mose cases, Pirkle's alcohol (**6**) revealed a higher activity (larger Δδ) as a CSA, possibly because of the increased acidity of the proton bond near the CF_3 group. Nevertheless, as we will see, the 3-D structure of the association complex could only be studied by intermolecular NOE in the case of compound **1**. Figure 1 shows a part of the NMR spectrum corresponding to the addition of 1.2 equiv of (*R*)-**1** to the racemic compound and to one enriched enantiomer of compound **3** (entries 2 and 3 in Table 1).

The chirality of all compounds tested was detected through NMR experiments, though the levels of discrimination varied greatly. Compound **2** showed the greatest difference in chemical shift between enantiomers. It seems that the presence of the nitrogen atom allows stronger intermolecular hydrogen bonds to form, which together with the π,π-stacking interactions constitutes the force enabling the chiral recognition (according to the model proposed by Pirkle and co-workers).[13]

Four samples were studied intenstively by NMR experiments: the two enantiomers of α-methylphenylacetic acid, **3**, with (*S*)-**1** (hereinafter called **S1S3** and **S1R3**) and the two enantiomers of 1-phenyl-1,2-ethanediol, **4**, with (*S*)-**1** (hereinafter called **S1S4** and **S1R4**). We first examined chemical shift changes between complexes. Tables 2 and 3 show the results of the NMR experiments. The difference in chemical shift for each enantiomer with respect to the free compound in the presence of any other compound was measured.

For compound **3**, induced chemical shifts on **S1S3** and **S1R3** were similar for the two enantiomers (0.01−0.03 ppm). The influence of the presence of the chiral reagent on compound **4** (**S1S4** and **S1R4**) was markedly different; the *S* enantiomer is shifted 0.09−0.12 ppm to high field, while the *R* enantiomer remained practically unmodified. Signals corresponding to compound **1** behaved similarly

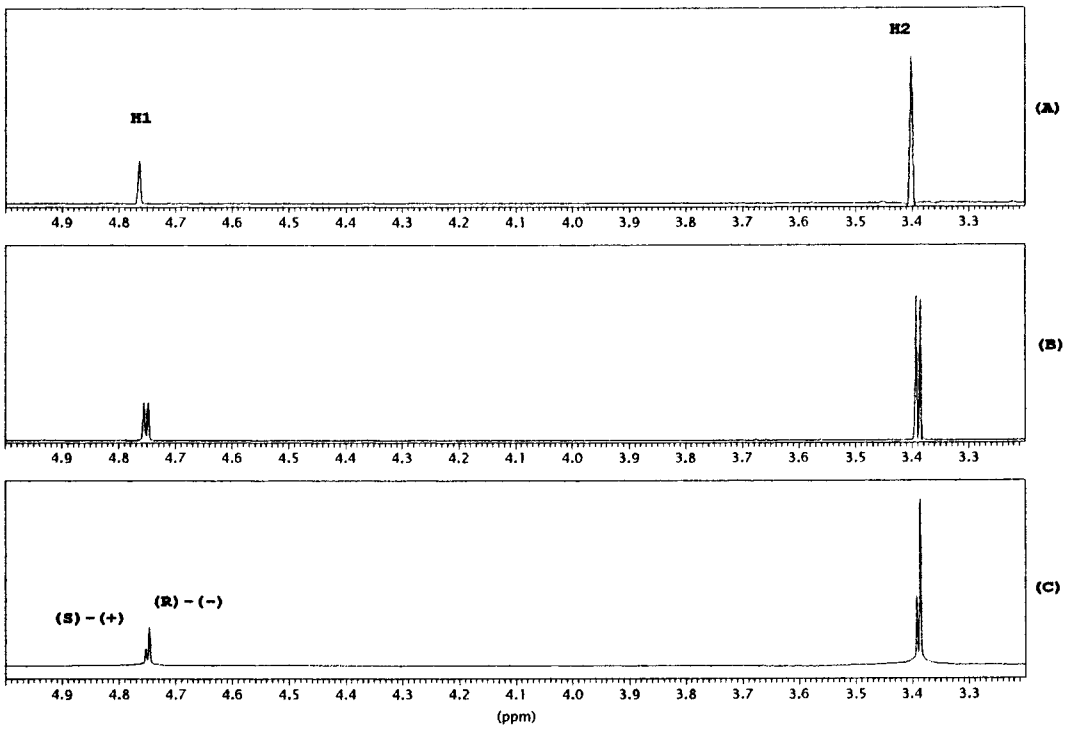

Figure 1. Aliphatic part of the NMR spectra of **3**: (A) pure **3**; (B) addition of (*R*)-**1** to racemic **3**; (C) addition of (*R*)-**1** to a one enantiomer enriched of **3**.

Table 2. Chemical Shift Changes (ppm) for 1:1 Mixtures of (*S*)-1 with Each Enantiomer of 3

		S1R3		S1S3	
proton	**1** or **3**	δ	$\Delta\delta$	δ	$\Delta\delta$
H_1-**1**	8. 32	8. 29	−0.03	8.28	−0.04
H_4-**1**	7. 99	7. 97	−0.02	7.99	0
H_5-**1**	7. 95	7. 93	−0.02	7.94	−0.01
H_8-**1**	9. 28	9. 26	−0.02	9.27	−0.01
H_{10}-**1**	8. 39	8. 36	−0.03	8.36	−0.03
H_{11}-**1**	6. 21	6. 19	−0.02	6.18	−0.03
H_{12}-**1**	1. 05	1. 05	0	1.05	0
H_1-**3**	4. 77	4. 76	−0.01	4.75	−0.02
H_2-**3**	3. 40	3. 39	−0.01	3.37	−0.03

Table 3. Chemical Shift Changes (ppm) for 1:1 Mixtures of (*S*)-1 with Each Enantiomer of 4

		S1R4		S1S4	
proton	**1** or **4**	δ	$\Delta\delta$	δ	$\Delta\delta$
H_1-**1**	8.32	8.32	0	8.29	−0.03
H_4-**1**	7.99	7.98	−0.01	7.96	−0.03
H_5-**1**	7.95	7.95	0	7.93	−0.02
H_8-**1**	9.28	9.27	−0.01	9.28	0
H_{10}-**1**	8.39	8.39	0	8.36	−0.03
H_{11}-**1**	6.21	6.2	−0.01	6.17	−0.04
H_{12}-**1**	1.05	1.05	0	1.05	0
H_1-**4**	4.79	4.79	0	4.67	−0.12
H_2-**4**	3.73	3.73	0	3.62	−0.11
H_3-**4**	3.62	3.63	0.01	3.53	−0.09

Table 4. Obtained NOE (%) in the 1:1 Mixtures of (*S*)-1 with Each Enantiomer of 3

saturated proton	S1R3	S1S3
H_8-**1**	H_1-**3** (5.3)	
H_{11}-**1**	H_1-**3** (2.2)	H_1-**3** (0.3)
H_{12}-**1**	H_1-**3** (1.3)	
H_1-**3**	H_{11}-**1** (12.5)	H_{11}-**1** (3.2)
H_1-**3**	H_8-**1** (11.2)	H_8-**1** (2.9)
H_2-**3**	H_{11}-**1** (5.6)	H_{11}-**1** (1.3)
H_2-**3**	H_8-**1** (4.7)	H-**1** (1.1)

Table 5. Obtained NOE (%) in the 1:1 Mixtures of (*S*)-1 with Each Enantiomer of 4

saturated proton	S1R4	S1S4
H_8-**1**		H_1-**4** (2.4)
H_8-**1**		H_2-**4** (3.2)
H_1-**4**	$H_{4,5}$-**1** (0.3/2)	
H_1-**4**	H_8-**1** (0.3)	H_8-**1** (0.5)
H_1-**4**	H_{11}-**1** (0.2)	H_{11}-**1** (0.5)
H_2-**4**		H_8-**1** (1.6)
H_2-**4**		H_{11}-**1** (2.2)

in both cases. These experimental results suggest that the complexation of the two enantiomers of **3** with (*S*)-**1** occurred in a similar way; unlike the two enantiomers of **4**. In other words, we can state with considerable certainly that the geometry and (or) the energy of the complex for **4** differ greatly for each isomer.

NOE Measurements. The same four samples from the intermolecular NOE experiments were studied using the NOEDIFF method. The results are summarised in Tables 4 and 5. The presence of intermolecular NOE values (Table 4) over H_8-**1** and H_{11}-**1**, on saturation of H_1-**3** and H_2-**3** (Figure 2), suggests that the complexes between **1** and **3** should have the cited protons close in the space. The relatively low intermolecular NOE values (0.2−3%) obtained between **1** and **4** suggest either a low association constant or a long distance between considered protons.

The NOE enhancements have also been studied in the complexes between Pirkle's alcohol (*S* enantiomer) and

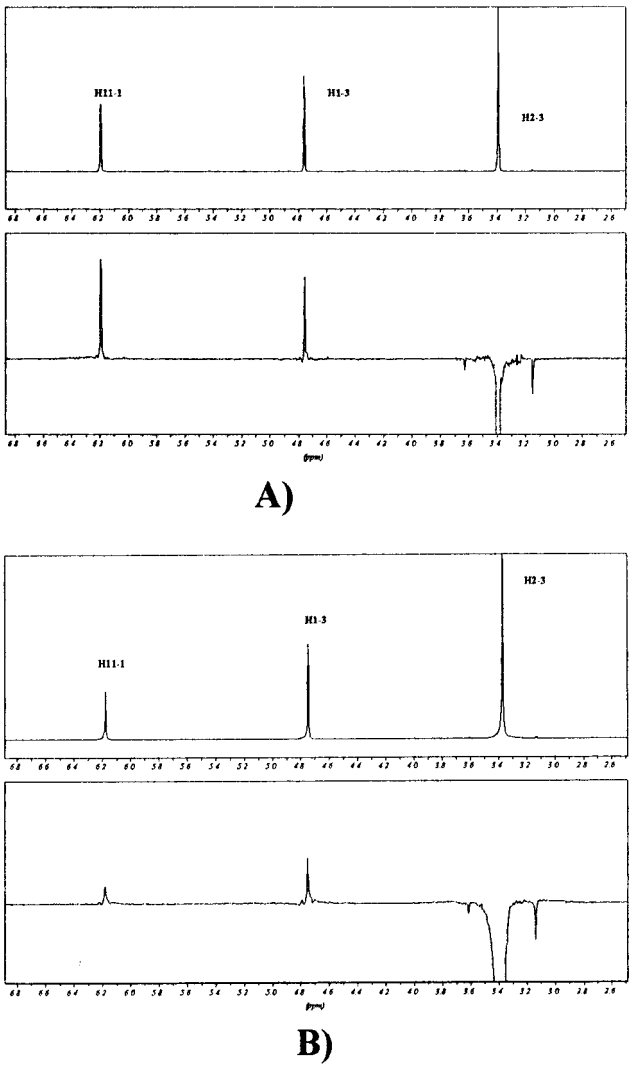

Figure 2. (A) Part of 300 MHz NMR spectrum of the **S1R3** complex (bottom) and the NOE difference spectrum after saturation of H_2-**3** (top). (B) Part of 300 MHz NMR spectrum of the **S1S3** complex (bottom) and the NOE difference spectrum after saturation of H_2-**3** (top).

Table 6. Obtained NOE (%) in the 1:1 Mixtures of (*S*)-6 with Each Enantiomer of 3

saturated proton	S6S3	S6R3
$H_{8/1}$-**6**	H_1-**3** (0.4)	H_1-**3** (0.3)
$H_{8/1}$-**6**	H_2-**3** (0.3/3)	H_2-**3** (0.3/3)
H_{11}-**6**	H_1-**3** (0.4)	H_1-**3** (0.8)
H_{11}-**6**	H_2-**3** (0.5/3)	H_2-**3** (0.7/3)
H_1-**3**	H_{11}-**6** (0.7)	H_{11}-**6** (0.5)
H_2-**3**	H_{11}-**6** (0.5)	H_{11}-**6** (0.3)

compounds **3** and **4** under similar conditions (Table 6). Weak NOEs are observed for the association with compound **3**, and an intermolecular NOE on the hydroxyl protons of **4** (2.5%) is transmitted only in the case[14] of saturation of H_{11}.

Molecular Dynamics Calculations. Molecular mechanics calculations (see Experimental Section) were carried out to find the most probable geometries for the complexes (Figure 3 a,b). These structures were used as starting points for the MD simulations.

Long molecular dynamics (MD) simulations (4500 ps) were carried out on the four complexes studied, **S1S3**, **S1R3**, **S1S4**, and **S1R4**, to ensure that all the conformational phase space for the system was covered.

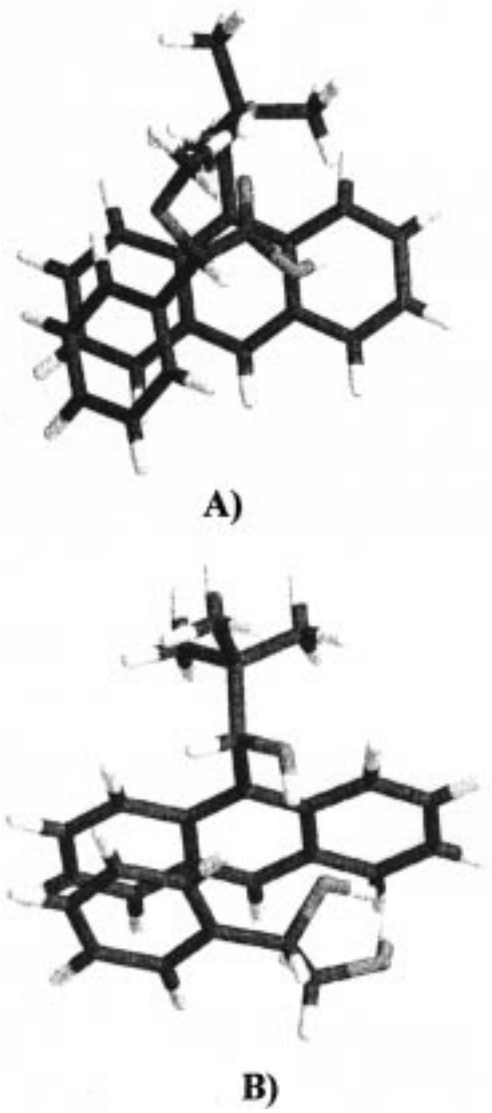

Figure 3. (A) Structure corresponding to the energy minimum for the **S1S4** complex as computed by AMBER* calculations. (B) Structure corresponding to the energy minimum for the **S1S3** complex as computed by AMBER* calculations.

Computed average energies indicate that complexes **S1S3** and **S1R3** are almost equally stable (total energies are 377.6 and 379.2 kJ/mol, respectively). Figure 4 contains plots of selected intermolecular distances versus simulation time (1500 ps) for **S1S3** and **S1R3**, as examples. Figure 5 contains plots for the accumulated average distance versus the simulation time. Runs longer than 2.5−3 ns are needed to ensure a stable average distance between intermolecular protons. Final averaged distances between H_8-**1**/H_1-**3** and H_{11}-**1**/H_1-**3** protons on both complexes are 5.340 and 5.090 Å for complex **S1S3** and 4.915 and 4.770 Å for complex S1R3.

Computed average energies for the MD runs of complexes **S1S4** and **S1R4** also indicate both complexes are nearly isoenergetic (total energies are 349.0 and 349.5 kJ/mol, respectively). Figure 6 contains plots of the selected intermolecular distances versus simulation time (1500 ps) for **S1S4** and **S1R4**, as examples. Figure 7 contains plots for the accumulated average distance versus the simulation time. Again, runs longer than 2.5−3 ns are needed to ensure a stable average distance between intermolecular protons. Final averaged distances between H_8-**1**/H_1-**4** and H_{11}-**1**/H_1-**4** protons on both complexes are 5.092 and 4.462 Å for complex **S1S4** and 4.637 and 4.759 Å for complex **S1R4**.

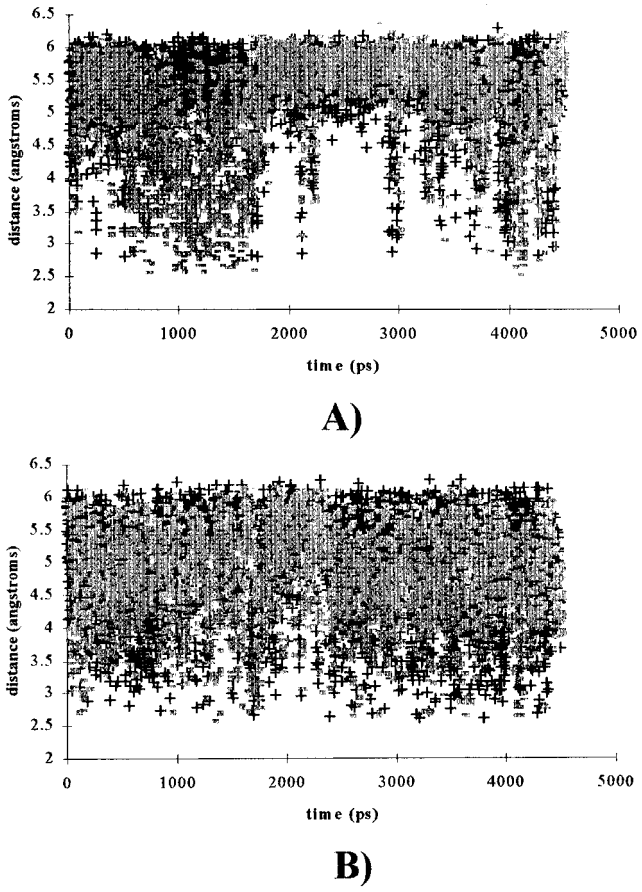

Figure 4. Plot of H_8-**1**/H_1-**3** (+) and H_{11}-**1**/H_1-**3** (□) distances versus simulation time (1500 ps): (A) complex **S1S3**; (B) complex **S1R3**.

An attempt to consider the rotational degrees of freedom over the complexes was carried out by performing stochastic dynamics calculations modeling the effect of the solvent (chloroform). Three rotatable torsion angles (one over molecule **1** and two over **3** or **4**) were allowed to change from +180° to −180°. No restrictions on the distance between molecules were introduced. Results from these computations indicate that molecules are near to each other only a few picoseconds at the beginning of the simulation. As soon as the benzylic bond of **1** rotates, both molecules start to separate and end at an infinite distance.

Discussion

Two differentials must be considered when dealing with NMR data. First, the cross-relaxation is a function of the distance in space between neighboring nuclei; the value of intermolecular NOE is obtained exclusively from the complex. Second, the magnetic influence of an aromatic system is considerable even at long distances between the π-system and the obseved nucleus; the obseved chemical shift is the average value of the chemical shift of the free species and that of the complex.

It is easily assumed that complexes involving Pirkle's alcohol, **6**, are highly stabilized by the hydrogen bond between the benzylic proton (H_{11}) and the oxygenated functions of **3** and **4**, in accordance the increased acidity

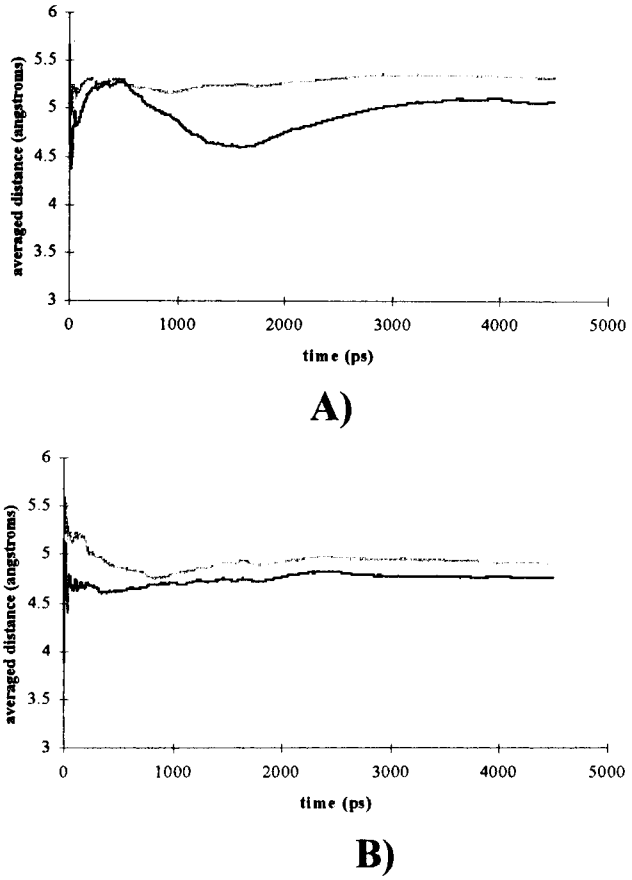

Figure 5. Plot for accumulated average distances between H_8-**1**/H_1-**3** and H_{11}-**1**/H_1-**3** protons versus simulation time (4500 ps): (A) complex **S1S3**; (B) complex **S1R3**.

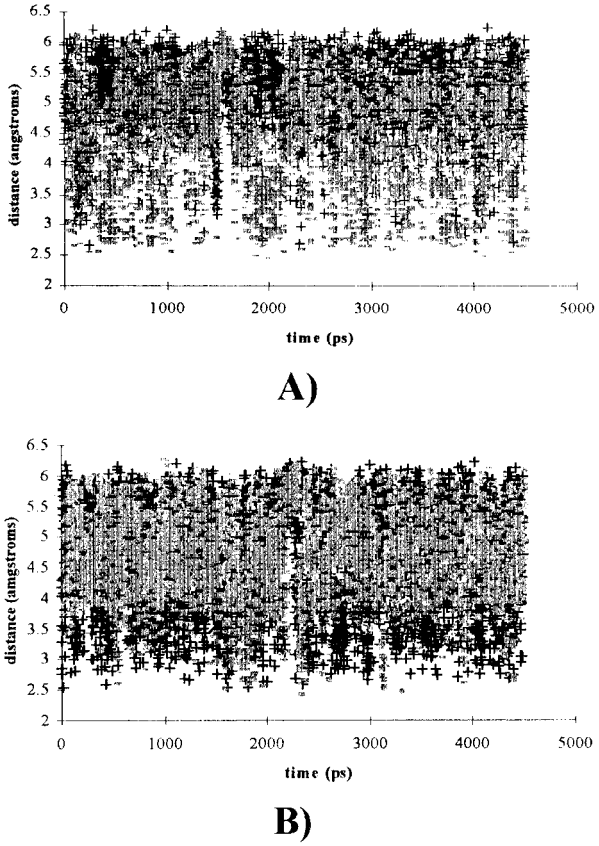

Figure 6. Plot of H_8-**1**/H_1-**4** (+) and H_{11}-**1**/H_1-**4** (□) distances versus simulation time (1500 ps): (A) complex **S1S4**; (B) complex **S1R4**.

of that proton. Thus, the complex formed does not need a very close approximation between atoms of the two molecules to gain stability. The lack of intermolecular NOEs is thus explained, and the observed shifts towards higher field are justified by the effect of the aromatic nucleus even at long distances.

In contrast to the Pirkle's alcohol behavior, the recognition process of our chiral compound **1** has to be quite different; experimental results included a weak shielding factor and important NOE values (Tables 4 and 5). Changes in chemical shift were negligible when (*S*)-**1** complexed with either enantiomer of compound **3**, and no discrimination between its enantiomers (Table 2) was detected. This fact indicates that the weight of the complexes in the observed chemical shift is low (i.e., low association constant or stability). However, the presence of important intermolecular NOE values (Table 4) over H_8-**1** and H_{11}-**1**, on irradiation of H_1-**3** and H_2-**3**, suggests that the geometry of the complexes between **1** and **3** is such that the cited protons are close enough in the space. Taking into account the experimental NOE values, the complex **S1R3** has either a longer life or a greater stability than the complex **S1S3**. In the association of **1** with **4**, the values of $\Delta\delta$ (Table 3) and the intermolecular NOEs (Table 5) indicate the formation of the solvating complex only in the case of **S1S4**.

Computed intermolecular distances between selected protons (H_8-**1**/H_1-**3**, and H_{11}-**1**/H_1-**3**) in complexes **S1S3** and **S1R3** were analyzed. Complex **S1S3** contains many structures having computed distances around 6 Å (Figure 4), while complex **S1R3** has significantly less structures trying to escape from close molecular contacts. Differences on computed average distances between these protons are, in consequence, significant and indicate that both independent molecules forming complex **S1R3** spend a longer time at a closer distance, in agreement with its larger experimental NOE (around 11%).

The MD runs for **S1S4** and **S1R4** complexes do not show any clear tendency to escape from close contacts (Figure 6); nevertheless, computed average distances between selected protons are different. The small NOE values experimentally observed (around 0.4%) prevent any comparison with computed distances.

Table 7 contains the energy distribution obtained in the MD calculations. Enantiodifferentiation is almost null for both pairs of studied diastereomeric complexes (less than 2 kJ/mole). As expected, energetic terms controlling intramolecular interactions are not crucial for the enantiodifferentiation, but the contribution of the long range interactions (electrostatic and van der Waals) has the largest influence over the final energy difference. Results from the stochastic dynamics suggest that inclusion of a solvation model diminishes the influence of the electrostatic term and molecules separate from each other. Conclusions extracted from geometric data should be thus more reliable than those from the energetic analysis.

Conclusions

The intermolecular NOEs were obseved for association complexes involving Pirkle-like chiral solvating agents and several aromatic substrates. Experimental data suggest highly different geometrical and energetic be-

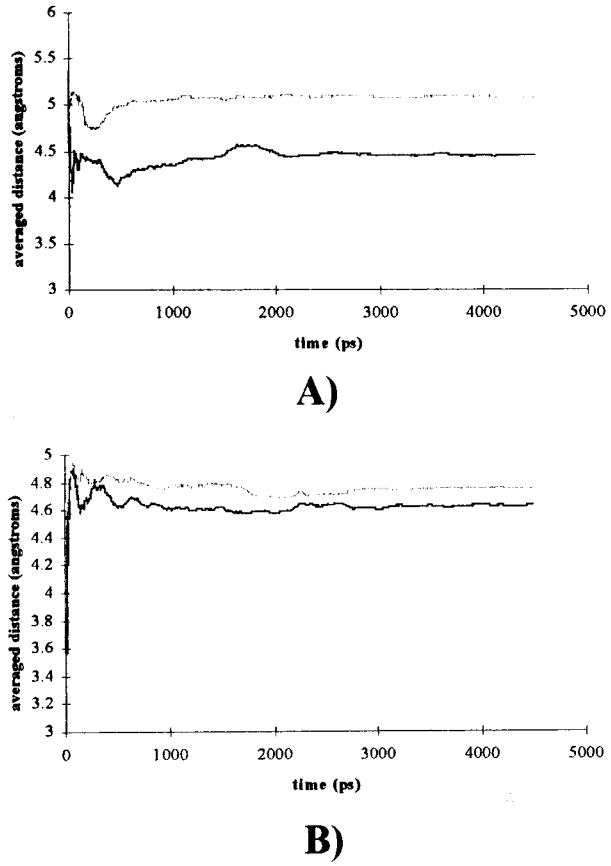

Figure 7. Plot for accumulated average distances between H_8-**1**/H_1-**4** and H_{11}-**1**/H_1-**4** protons versus simulation time (4500 ps): (A) complex **S1S4**; (B) complex **S1R4**.

havior between Pirkle's alcohol and our related substrates. While Pirkle's alcohol forms stable complexes with separated molecules (no intermolecular NOE observed), compound **1** does not produce very stable complexes but has much closer atomic contacts between individual components (intermolecular NOE observed). Molecular dynamics calculations, which correctly indicated the relative proximity between protons in the diastereomeric complexes studied, are of help in assessing the main driving forces behind complex formation and eventually for the enantiodifferentiation process.

Experimental Section

NMR Experiments. NMR experiments were conducted at 300 K on a Bruker DPX-300 or a Bruker ARX-400, using Cl_3-CD as the solvent. All steady-state NOE experiments were obtained using a 0.4 M solution of each complex that was degassed by three freeze−thaw−pump cycles and then sealed. The conditions used were as follows: 8 s of low power presaturation with a filter corresponding to a ±30 Hz width, spectrum window 12 ppm, two dummy scans, number of scans = 8, number of cycles = 10−40 (depending of the signal-to-noise ratio).

Computational Method. Conformational analyses were performed on isolated molecules. The most stable conformer was used in the next steps of this study. The approximation of substrates to (*S*)-**1** was emulated following a method similar to one previously published.[15] Molecule (*S*)-**1** was situated at the origin of the coordinates. The substrates were located at

(15) Lipkowitz, K. B.; Demeter, D. A.; Zegarra, R.; Larter, R.; Darden, T. *J. Am. Chem. Soc.* **1988**, *110*, 3446. (b) Lipkowitz, K. B.; Baker, B.; Zegarra, R. *J. Comput. Chem.* **1989**, *10*, 718.

Table 7. Energy Distribution (kcal/mol) For the Studied Complexes As Obtained by the MD Calculations

	S1R3			S1S3			ΔE S1R3 − S1S3	S1R4			S2S4			ΔE S1R4 − S1S4
conf[a]	1	2	3	avg	1	2	3	avg		1	2	3	avg	1	2	3	avg	
PE	233.64	237.27	235.42	235.44	234.53	230.42	235.74	233.56	1.88	208.93	212.30	210.84	210.69	210.18	209.53	210.60	210.10	0.59
stret	13.33	13.67	13.52	13.51	13.59	13.64	13.59	13.61	−0.10	12.73	12.85	12.90	12.83	13.15	12.83	13.18	13.05	−0.22
bend	107.65	107.45	108.44	107.85	107.25	107.59	107.71	107.52	0.33	103.98	103.68	103.46	103.71	103.75	103.42	103.80	103.66	0.05
tors	60.39	59.62	62.81	60.94	61.62	61.67	62.29	61.86	−0.92	58.04	58.02	57.96	58.01	57.90	59.20	57.53	58.21	−0.26
vdW	50.35	52.16	48.92	50.48	51.91	50.64	51.62	51.39	−0.91	52.23	54.21	53.33	53.26	52.93	52.53	53.35	52.94	0.32
elect.	1.92	4.37	1.73	2.67	0.17	−3.12	0.53	−0.81	3.48	−18.05	−16.47	−16.82	−17.11	−17.55	−18.45	−17.26	−17.75	0.64

[a] Three conformations were considered as a starting point for each studied complex (see Experimental Section for more details).

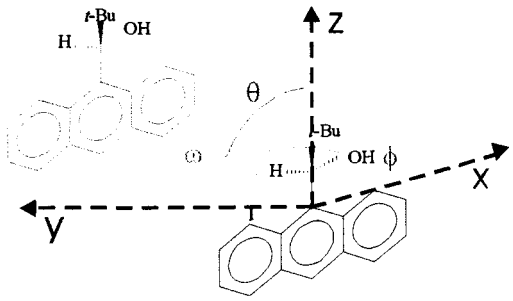

Figure 8. Geometric parameters used for covering all the space around the Pirkle-like alcohol in the AMBER* molecular mechanics calculations.

different places around (*S*)-**1** by changing its spherical coordinates θ and ϕ, while r was set to 7 Å. For each of these points, a rotation around the axis formed by the two molecules (ω) and an optimization of the distance between them was carried out (see Figure 8). Structures corresponding to the lowest energy minimum of each rotation were collected and used to draw a potential energy surface as a function of θ and ϕ. All local minima were reoptimized again without any restraint.

Molecular mechanics calculations were performed on SGI INDY workstations using the AMBER all-atom force field[16] as implemented in the version 5.0 of the MacroModel[17] and BatchMin packages (called AMBER*). The Polak−Ribiere[18] conjugate gradient minimizer was used. Cut-off values have been extended to 8 Å for van der Waals and to 20 Å for electrostatic interactions. No solvent model was employed, and the default dielectric constant was used.

Molecular dynamics calculations were carried out on a SGI Power Challenge computer using the AMBER all-atom force field[16] as implemented in the version 5.0 of the MacroModel and BatchMin packages.[17] The temperature was fixed at 298 K. Electrostatic interactions were estimated with the default dielectric constant. Extended nonbonded cut-off distances were set to 15 Å for the van der Waals and electrostatic interactions. Distance constraints (flat-bottom type, 500 kJ/mol, 6 Å > d > 3 Å) between selected protons (H_8 and H_{11} for (*S*)-**1** and H_1 for **3** and **4**) were applied to better simulate the experimental NOE values. The three most stable geometries coming from the MM calculations were used as starting points. MD simulations were run for 1500 ps using a time step of 1 fs, giving a total of 4500 ps for each studied complex.

Stochastic dynamics calculations (1000 ps) were performed using the AMBER all-atom force field[16] as implemented in the version 5.0 of the MacroModel and BatchMin packages.[17] The presence of the solvent ($CHCl_3$) was modeled ujsing the GB/SA solvation model.[19] Configurations were produced by changing three torsion angles (C═C−C−O in **1**, C═C−C−O and C−C−O−Me in **3**, or C═C−C−O and O−C−C−O in **4**), and one torsional change was allowed at each MD step.

Acknowledgment. Financial support was received from DGICYT (Projects PB95-0636 and PB96-1181). CIRIT and UAB are gratefully acknowledged for fellowships (M. de M. and E.C., respectively). We thank the Servei de Ressonància Magnètica Nuclear of UAB for allocating spectrometer time. Part of this research has been carried out using the CESCA-CEPBA computers. C[4] is gratefully acknowledged for allocating computing time.

JO980261F

(16) (a) Weiner, S. J.; Kollman, P. A.; Case, D. A.; Singh, U. C.; Chio, C.; Alagona, G.; Profeta, S.; Weiner, P. *J. Am. Chem. Soc.* **1984**, *106*, 765. (b) Weiner, S. J.; Kollman, P. A.; Case, D. A. *J. Comput. Chem.* **1986**, *7*, 230.

(17) Mohmadi, F.; Richards, N. G. J.; Guida, W. C.; Liskamp, R.; Lipton, M.; Caufield, C.; Chang, G.; Hendrickson, T.; Still, W. C. *J. Comput. Chem.* **1990**, *11*, 440.

(18) Polak, E.; Ribiere, G. *Rev. Fr. Inf. Rech. Oper.* **1969**, *16−R1*, 35.

(19) Still, W. C.; Tempczyk, A.; Hawley, R. C.; Hendrikson, T. *J. Am. Chem. Soc.* **1990**, *112*, 6127.